NASA Technical Memorandum 102069

Two-Dimensional Analysis of Two-Phase Reacting Flow in a Firing Direct-Injection Diesel Engine

H. Lee Nguyen
Lewis Research Center
Cleveland, Ohio

December 1989

NASA

TWO-DIMENSIONAL ANALYSIS OF TWO-PHASE REACTING FLOW IN A FIRING DIRECT-INJECTION DIESEL ENGINE

H. Lee Nguyen
National Aeronautics and Space Administration
Lewis Research Center
Cleveland, Ohio 44135

SUMMARY

This report describes a study of the flow field, spray penetration, vaporization, and combustion in two-stroke diesel engines. Fuel injection begins at 345° after top dead center (ATDC), and n-dodecane is used as the liquid fuel. Arrhenius kinetics is used to calculate the reaction rate term in the quasi-global combustion model. When the temperature, fuel, and oxygen mass fraction are within suitable flammability limits, combustion begins spontaneously. No spark is necessary to ignite a localized high-temperature region. Compression is sufficient to increase the gaseous phase temperature to a point where spontaneous chemical reactions occur. Results are described for a swirl angle of 22.5°.

INTRODUCTION

This report describes the flow field, spray penetration, vaporization and mixing, and combustion in a two-stroke diesel engine. This study of the firing diesel engine uses the same geometry, initial conditions, and boundary conditions as were used for the motored case studied previously (ref. 1). Liquid spray combustion begins at 345° after top dead center (ATDC) (end of compression stroke) when fuel injection begins. The Eulerian conditions of the gas phase are identical to those used in the motored case (ref. 1) and are not repeated here. The initial conditions of the liquid phase are also the same as those used in the motored case but they are repeated in the next section. Arrhenius kinetics is used to calculate the reaction rate term. The results show the firing cycle to be composed of three periods: (1) ignition delay, (2) explosion, and (3) controlled diffusive burning. The ignition delay period is characterized by fuel vaporization and extensive mixing in an envelope around the spray. Explosive combustion begins abruptly throughout the partially premixed envelope once the temperature of the engine cylinder rises to within the fuel flammability limits. Large pressure gradients and pressure-driven flow dominate the combustion and droplet dynamics during the explosion, resulting in rapid droplet vaporization and dispersion. Large regions of fuel vapor develop near the injector. After a short period of explosive premixed burning, more controlled diffusion fuel flames develop. Vortices generated by the injection of liquid fuel and by several localized combustion regions partially mix the segregated regions of fuel and oxygen. During expansion, large-scale vortices gradually decay as piston-driven flow develops. Although localized combustion continues throughout the expansion stroke, insufficient large-scale motion results in incomplete mixing of the fuel and oxygen.

PROBLEM FORMULATION

The piston-cylinder configuration analyzed herein consists of a (1) circumferential intake port located at the cylinder wall that is covered and uncovered by the piston; (2) an infinitesimally thin exhaust valve, which is located at the center of the cylinder head and penetrates the cylinder at specified crank angles; and (3) an injector located at the cylinder centerline and cylinder head (refs. 1 to 3). The geometric characteristics of this two-stroke diesel engine are presented in figure 1.

Descriptions of the mean flow field, the two-equation model of turbulence, and the discrete droplet model can be found in references 1 to 3. A one-step irreversible chemical reaction of the Arrhenius type is used to model the conversion of fuel ($C_{12}H_{26}$) and oxidizer (O_2) into combustion products (CO_2 and H_2O). The Arrhenius kinetics oxidation reaction rate was assumed to be proportional to a temperature-activated exponential term; the values of the pre-exponential factor, the activation energy, the powers of fuel, and oxidizer concentrations are taken from reference 4.

PRESENTATION AND DISCUSSION OF RESULTS

Table I summarizes the engine variables investigated in this report. The firing study uses the same geometry, initial conditions, and boundary conditions as were used by the motored case. The compression period is identical to that of the motored case (refs. 1 to 3) and is not repeated here. The study begins at 345° ATDC with the beginning of fuel injection; the final output of the compression stage is read and used as the initial conditions.

Three distinct combustion periods exist in the cylinder during one cycle. The first period, commonly called the ignition delay period, lasts from 345° ATDC until approximately 353° ATDC for the geometry being modeled at 1000 rpm; the length, however, changes significantly depending on rpm, geometry, intake boost, compression ratio, etc. During this time the liquid fuel vaporizes as it did in the motored study; however, combustion is insignificant because of the lack of energy to initiate the chemical reaction. Two effects cause the delay - (1) the vaporization cooling of the regions of partially mixed fuel and oxygen and (2) the insufficient compression of the cylinder gases. During this period significant regions of nearly stoichiometric mixture develop in an envelope around the spray region. Gradually compression and heat transfer from the warmer regions raise the temperature of these regions giving rise to the second period.

An explosive situation exists for about 2° when the temperature of the partially premixed region initiates a rapid combustion. The combustion quickly consumes the partially premixed fuel in the envelope around the liquid fuel. Rapid pressure and temperature rises occur throughout the cylinder. After all the initially short premixed regions have been burned, the combustion relaxes into the third period.

This third combustion period is characterized by diffusion-controlled flames. The gaseous fuel is located primarily in the injector region, near the injection vortex, where the droplets vaporized. The oxygen is located around the fuel-rich region, throughout the rest of the cylinder. Combustion proceeds but at a relatively slow rate as the fuel and oxygen diffuse

together. A diffusion flame envelopes the fuel-rich center and slow and more controlled combustion continues until the blow-down period begins.

Figures 2 to 4 show the ignition delay period. Figures 2 and 3 show the velocity, fuel, oxygen, and carbon dioxide plots at 350° ATDC. Figure 2 shows the development of the injection-driven vortex and the scraping vortex along the cylinder wall. The major feature in the flow is the momentum exchange between the liquid and gaseous phases. Figure 3 shows the localized region of gaseous fuel mass. Fuel displaces the oxygen near the injector. Note that no appreciable combustion occurred anywhere in the cylinder (fig. 3).

Figures 4 and 5 show the hydrodynamic features at the last instant before the explosion period begins. The velocity in the injection vortex (fig. 4) is well developed as the liquid-gas momentum transfer drives the flow. In figure 5, the effects of vaporization cooling are seen near the injector. The temperature is uniform throughout the cylinder with sharp temperature gradients near the walls.

Figures 6 and 7 show the crankshaft degree during which explosive combustion is present in the chamber. These figures also show the velocity, temperature, pressure, carbon dioxide, oxygen, and fuel at 355° ATDC. Figure 7 shows a nearly unidirectional velocity field during the explosion. No injection or scraping vortex can be seen as the explosive pressure rise drives all aspects of the flow. Figure 7 shows the temperature rises in the cylinder. A large, partially premixed region located near the cylinder head at the interface between the gaseous fuel and oxygen explodes, causing a rapid temperature rise in that region. Note the relatively large region over which temperature has increased, indicating a large amount of burning and, also, that a large amount of partially premixed fuel and oxygen was present at 354° ATDC. Large pressure gradients exist between the cylinder wall and the centerline, and the global pressure in the cylinder has increased by a factor of three. The carbon dioxide is a major combustion product in the burned region near the injector. The fuel air mixture originally associated with the injection vortex was premixed to within the flammability limits of the fuel and burned during the explosion period. Levels of oxygen near the injector are substantially reduced, and most of the gaseous fuel outside the dense liquid spray core region is consumed in the explosion. This explains the large region over which a substantial temperature rise was observed (fig. 7). The regions near the cylinder wall where no combustion is present increase in temperature due to the adiabatic compression associated with the large cylinder pressure rise.

Figures 8 and 9 show the velocity and temperature profiles, respectively, at 356° ATDC. Small effects of the explosion period can still be seen here. Figure 8 shows a nearly unidirectional rebound from the cylinder wall toward the centerline. A small injection vortex is still observed near the injector region, and recirculation regions are present when the flow strikes the centerline as well as in the regions near the cylinder wall. Figure 9 shows that further burning near the centerline occurs.

After a short period of 2° of explosive premixed combustion, the burning slows into diffusion-controlled combustion. Figures 10 and 11 show the velocity and temperature, respectively, at 357°. Figure 10 shows the development of two large combustion-driven vortices and the redevelopment of the

injection vortex. One vortex is located on either side of an interface line dividing the fuel-rich center from the oxygen-rich region of the cylinder. The fuel-side vortex is driven by the combustion near the piston face. Figure 11 shows the region near the piston face that is burning. The remains of the large premixed regions near the center of the cylinder are burning and drive the two large recirculation zones.

Figures 12 to 15 show the velocity, temperature, and carbon dioxide plots at 358° and 359°. The velocity plots indicate the further development of the injection-driven vortex. The temperature profiles indicate burning in the injection vortex near the centerline and at the interface between the oxygen and fuel vortices near the cylinder head.

Figures 16 to 18 show the velocity, temperature, carbon dioxide, oxygen, and fuel profiles at 360° ATDC. Figure 16 shows the continuing development of the injection-driven vortex. The temperature profile (fig. 17) shows only weak combustion near the injection-driven vortex. Figure 18 shows the reason for the lack of combustion. The fuel located predominantly near the injection vortex is gradually drawn into the vortex located in the fuel-rich region. The oxygen is located primarily near the vortex located in the oxygen-rich region. In figure 18, the result of the combustion can be seen near the cylinder head next to the oxygen-rich region where the oxygen is depleted and the carbon dioxide is abundant. This explains the high-temperature region that is present in the cylinder head near the oxygen-rich region.

Figures 19 to 22 show the velocity profiles at 1° to 4° ATDC, respectively. The velocity near the injector develops into a strong injection-driven vortex. Both combustion-driven vortices decay substantially, and combustion has effectively stopped.

Figures 23 and 24 show the velocity and temperature at 5° ATDC. The velocity profiles show that on the last degree of injection the liquid momentum-driven injection vortex is again established and is driving the flow in the region near the injector. Combustion is nearly extinguished and no longer drives the mixing of fuel and oxygen. The temperature profile indicates oxygen-rich outer regions and fuel-rich center regions. Correspondingly, the temperature is hottest at the interface and cooler on each side. The oxygen-rich region is cooler since no combustion has occurred there. There are no large-scale motions that are mixing the fuel with the oxygen. The fuel is swept into the center of the cylinder by the injection vortex but most never reaches the oxygen-rich region.

Injection ends at 5° ATDC, and the injection-driven vortex moves more toward mid-cylinder. Figures 25 and 26 show the velocity and temperature profiles at 10° ATDC. The injection vortex has adjusted itself to the lack of droplets near the injector, and there are indication of the piston beginning to drive the flow. Both the fuel-rich region and oxygen-rich side vortices are stretched by the presence of the injectors vortices. Rapid expansion away from the burning causes a separation in the flow (fig. 25). A rise in temperature develops near the cylinder head causing new combustion near the cylinder head (fig. 26).

Figures 27 and 28 show the previously mentioned variables at 15° ATDC. Figure 27 shows the piston beginning to drive the flow. The combustion

present at 10° ATDC has decayed. Figure 28 shows a temperature peak near the center of the cylinder where combustion raises the gaseous temperature. Boundary layers are developing along the three walls. No large-scale motion exists to mix the separated fuel and oxygen.

Figures 29 and 30 show the previously mentioned variables at 20° ATDC. The piston drives the flow throughout most of the cylinder, and the injection vortex is somewhat diminished. Near the cylinder wall a new region of combustion occurs (near the middle of the plot). Figure 30 shows a localized high-temperature region.

Figures 31 and 32 show the flow patterns at 30° ATDC. Figure 31 shows a nearly piston-driven flow with the remains of the injection vortex. The cylinder head side of the vortex carries small amounts of fuel into the oxygen-rich outer regions. A localized temperature spike in figure 32 shows the presence of combustion. Gradually fuel diffuses into the middle regions of the cylinder that were once occupied solely by combustion products.

Figures 33 and 34 show flow patterns at 40° ATDC, similar to those described at 30° ATDC. The remains of the injection vortex carry fuel along the cylinder head into the oxygen-rich region causing localized combustion regions.

Figures 35 to 40 show the previously mentioned variables at crankshaft angles of 60°, 80°, and 108°. Figures 35, 37, and 39 show a gradual increase in the degree the piston dominates the flow. The remains of the injection vortex still move fuel along the cylinder head into the oxygen-rich outer regions. The temperature plots (figs. 36, 38, and 40) show the presence of small-scale combustion along the cylinder head. Gradually the flame front moves radially with the injection vortex. At 108° ATDC, the flow is nearly unidirectional. No large-scale motions present in the cylinder are capable of completely mixing the remaining fuel and oxygen.

Approximately the last 88° (20° to 108° ATDC) show very similar behavior. Gradually the piston begins to drive the flow in a unidirectional manner. Only one vortex persists, the injection vortex, and it gradually moves fuel from the fuel-rich center region toward the oxygen-rich outer cylinder along the cylinder wall. The temperature in the cylinder slowly decreases due to adiabatic expansion except for localized regions of combustion near the cylinder head. Gradually thermal boundary layers form as heat is lost to the cylinder walls.

Figures 41 to 45 show plots of the turbulent kinetic energy at 350°, 360°, 10°, 40°, and 108° ATDC, respectively. Figure 41 shows the turbulence levels before the beginning of combustion. Nearly uniform levels of turbulence exist throughout the cylinder except near the injector, where the injection process generates levels of turbulence an order of magnitude larger than the background levels.

Figure 42 shows the turbulence levels immediately after the explosion premixed combustion period at 360° ATDC. As in figure 42, the presence of three vortices is clearly seen as the local levels of turbulence increase in the shear layers associated with the three vortices. These levels are an

order of magnitude larger than the background levels. Figure 43 shows the turbulence at 10° ATDC. The injection vortex and the oxygen-rich-region vortex still are strong enough to generate turbulence but global levels decay. Figures 44 and 45 show the turbulence levels at 40° and 108° ATDC, respectively. No substantial large-scale motion generates turbulence in the cylinder, and levels are nearly uniform throughout the cylinder. Only near the walls can turbulence generation be observed.

Figure 46 shows the dissipation rate of turbulent kinetic energy at 350° ATDC. Inspection of this figure indicates that the dissipation rate mimics the turbulent kinetic energy level. Large levels of turbulence produce large dissipation rates.

CONCLUSIONS

Calculations of the firing two-stroke diesel engine for a 22.5° swirl angle were reported, and some conclusions can be summarized as follows:

1. During the initial period of the combustion cycle (ignition delay period), hydrodynamics controls the flow which is primarily driven by the injection vortex. Large regions of partially premixed fuel are formed around the liquid spray region. Vaporization cooling keeps combustion from immediately occurring in these regions.

2. Explosive premixed combustion occurs throughout a large portion of the cylinder once combustible temperatures are achieved in the cylinder due to compression of the gases by the piston and the local fuel/air ratio are within the flammability limits. This period lasts from 8° to 10° ATDC.

3. Large-scale pressure gradients drive the flow immediately after the explosive premixed combustion period. The large flow velocities quickly disperse the remaining droplets throughout the cylinder.

4. Large temperature rises in the cylinder quickly vaporize a large percentage of the droplet mass which creates (in this geometry) large fuel-rich regions near the cylinder centerline. These fuel-rich regions slowly move and diffuse toward the oxygen-rich region located near the cylinder wall.

5. After the explosive period, a diffusion-controlled combustion period begins in which injected fuel drives the flow near the injector and fuel and oxygen move and diffuse together as a result of large-scale fluid motion. Diffusion-controlled combustion continues to occur in localized regions throughout the cylinder for the remainder of the expansion stroke.

REFERENCES

1. Nguyen, H.L., et al.: Numerical Simulation of the Flow Field and Fuel Sprays in an IC Engine. SAE Paper 870599, 1987.

2. Nguyen, H.L.; Carpenter, M.H.; and Ramos, J.I.: The Effects of Engine Speed and Injection Characteristics on the Flow field and Fuel/Air Mixing in Motored Two-Stroke Diesel Engines. AIAA Paper 87-0227, 1987.

3. Carpenter, M.H.: A Numerical Simulation of the Direct Injection Diesel Engine under Motored and Firing Conditions. Ph.D Thesis, Carnegie-Mellon University, Pittsburgh, PA, 1986.

4. Westbrook, C.K.; and Dryer, F.L.: Chemical Kinetic Modeling of Hydrocarbon Combustion. Progress in Energy and Combustion Science, vol. 10, 1984, pp. 1-57.

TABLE. I. - ENGINE VARIABLES INVESTIGATED

Speed, rpm	Swirl angle, deg	Spray angle, deg	Injection angle, deg ATDC	Peak of droplet distribution function, d_{peak}, mm	Maximum droplet diameter, d_{max}, mm
1000	22.5	78	345	30.8	50

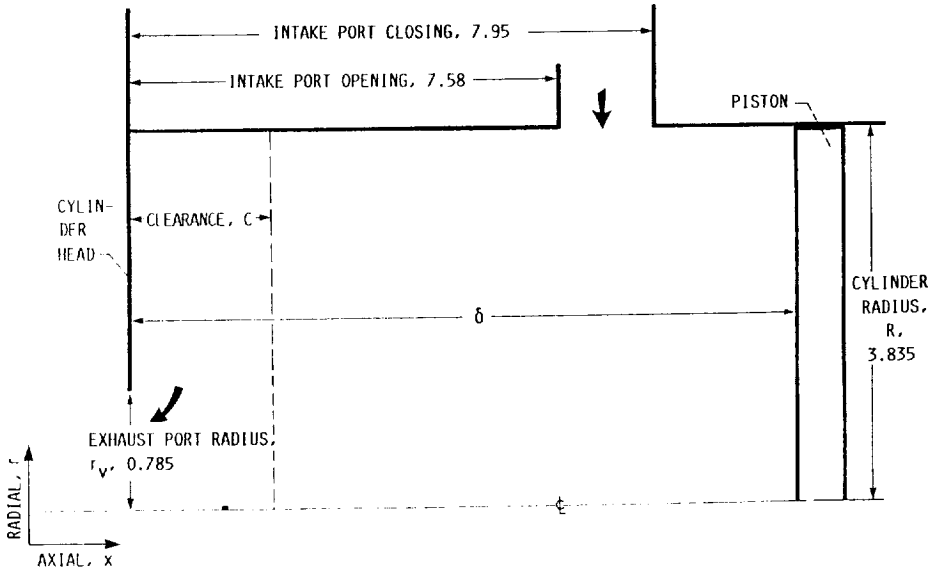

FIGURE 1. - GEOMETRY OF DIESEL ENGINE CHAMBER. (ALL DIMENSIONS ARE IN INCHES.)

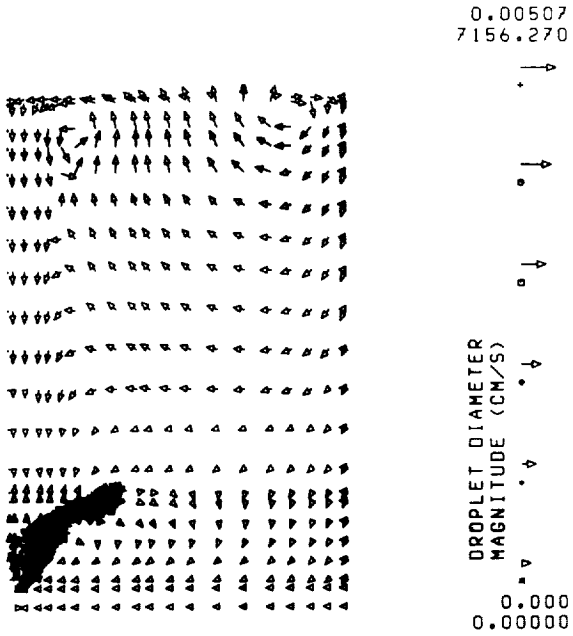

FIGURE 2. - GAS PHASE VELOCITY VECTOR PROFILES AND DROPLET LOCATIONS AT 350° ATDC FOR 22.5° SWIRL ANGLE.

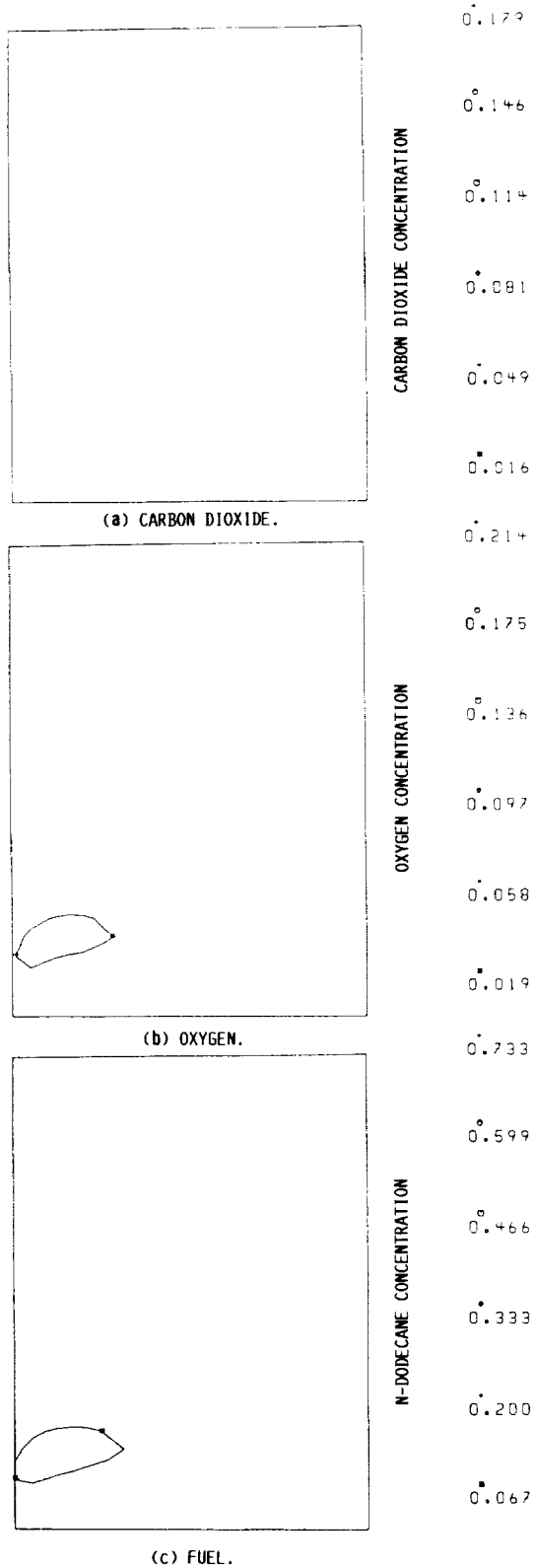

FIGURE 3. - MASS FRACTION DISTRIBUTIONS AT 350° ATDC FOR

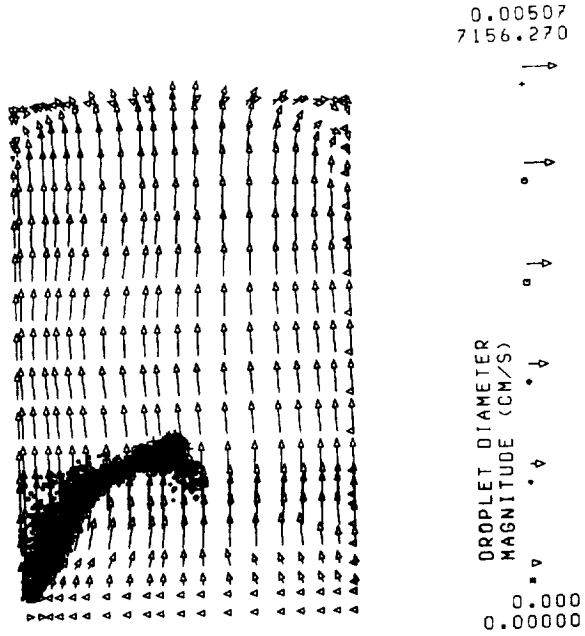

FIGURE 4. - GAS PHASE VELOCITY VECTOR PROFILES AND DROPLET LOCATIONS AT 354^{0} ATDC FOR 22.5^{0} SWIRL ANGLE.

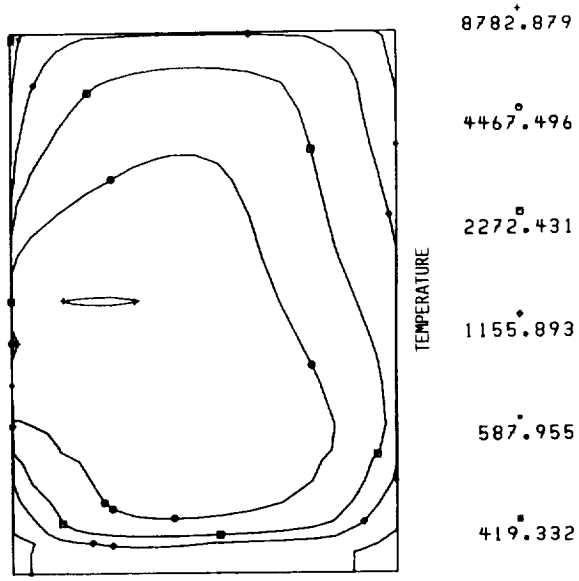

FIGURE 5. - TEMPERATURE ISOCONTOURS AT 354^{0} ATDC FOR 22.5^{0} SWIRL ANGLE.

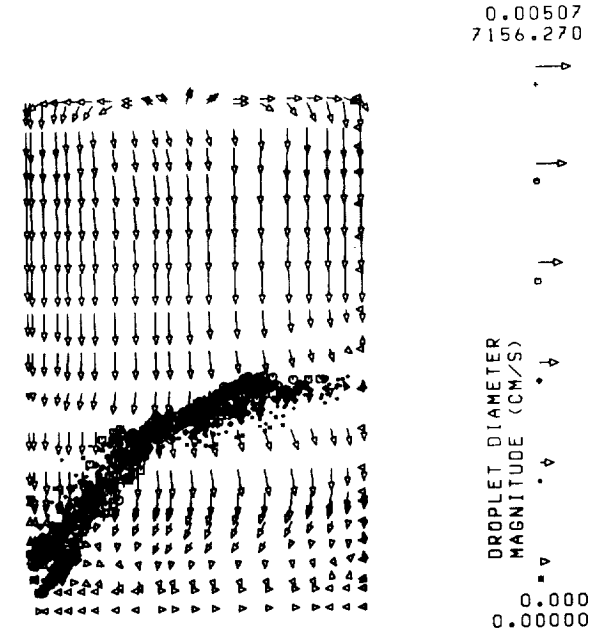

FIGURE 6. - GAS PHASE VELOCITY VECTOR PROFILE AND DROPLET LOCATIONS AT 355^{0} ATDC FOR 22.5^{0} SWIRL ANGLE.

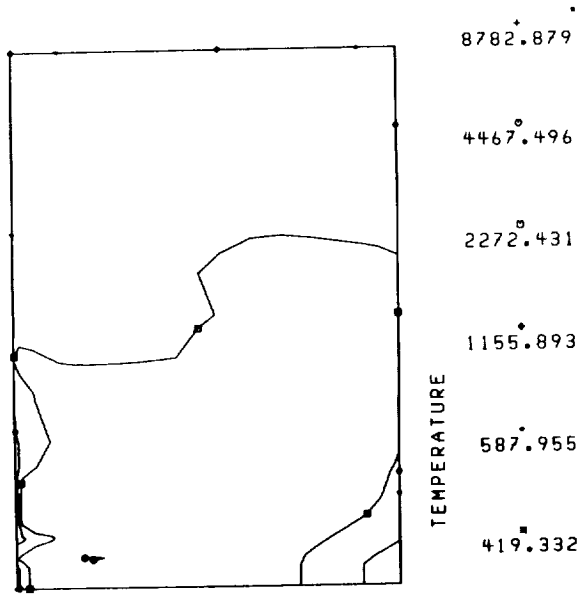

FIGURE 7. - TEMPERATURE ISOCONTOURS AT 355^{0} ATDC FOR 22.5^{0} SWIRL ANGLE.

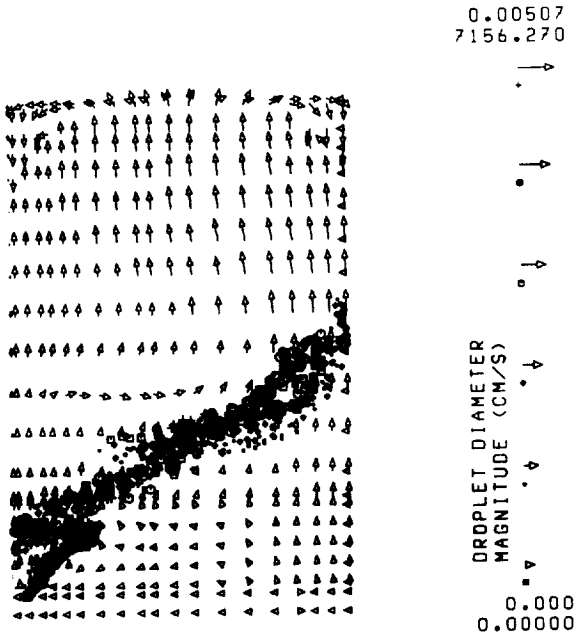

FIGURE 8. - GAS PHASE VELOCITY VECTOR PROFILES AND DROPLET LOCATIONS AT 356^{0} ATDC FOR 22.5^{0} SWIRL ANGLE.

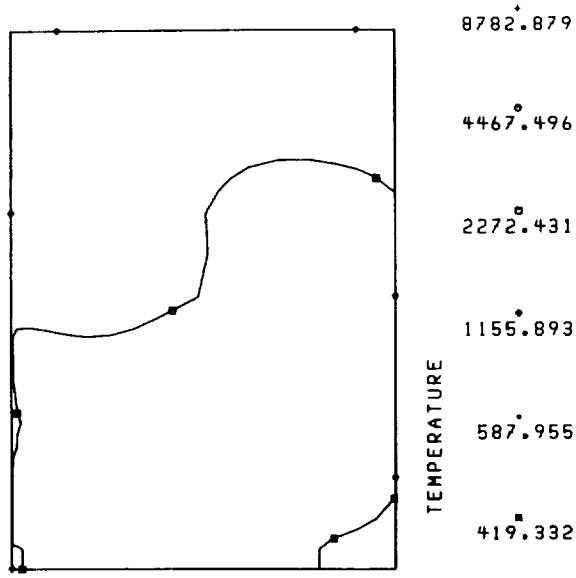

FIGURE 9. - TEMPERATURE ISOCONTOURS AT 356^{0} ATDC FOR 22.5^{0} SWIRL ANGLE.

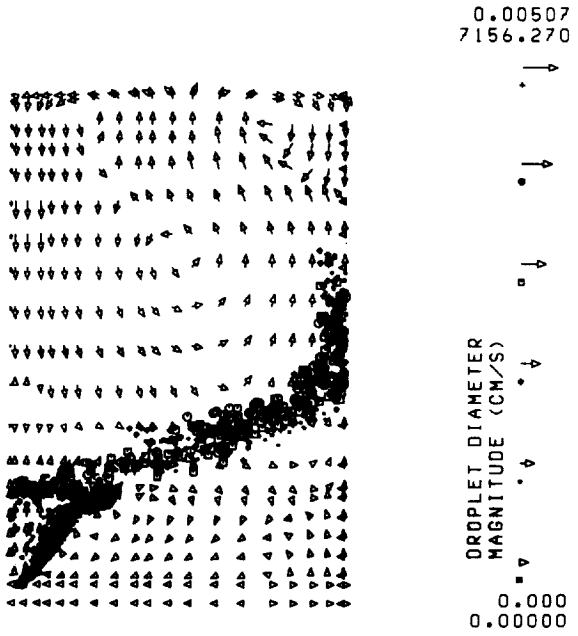

FIGURE 10. - GAS PHASE VELOCITY VECTOR PROFILES AND DROPLET LOCATIONS AT 357^{0} ATDC FOR 22.5^{0} SWIRL ANGLE.

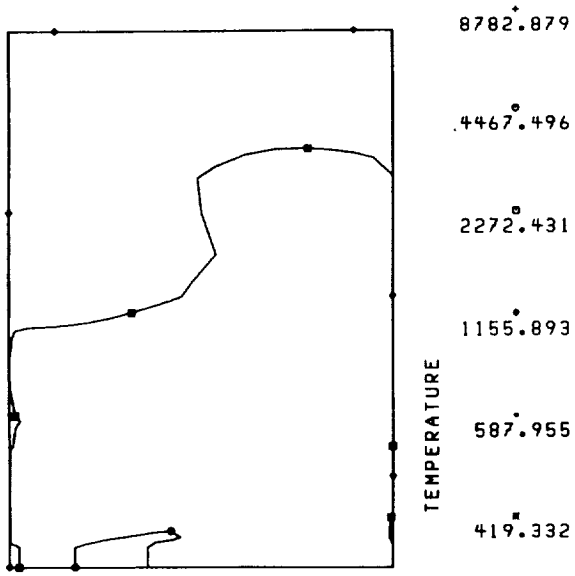

FIGURE 11. - TEMPERATURE ISOCONTOURS AT 357^{0} ATDC FOR 22.5^{0} SWIRL ANGLE.

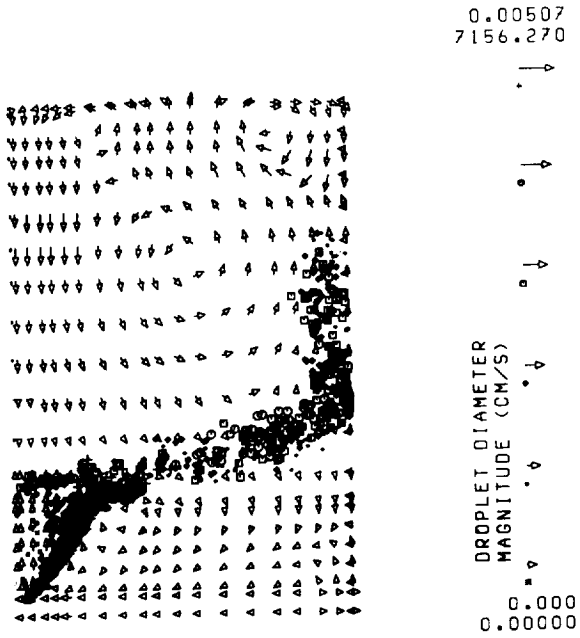

FIGURE 12. - GAS PHASE VELOCITY VECTOR PROFILES AND DROPLET LOCATIONS AT 358^{0} ATDC FOR 22.5^{0} SWIRL ANGLE.

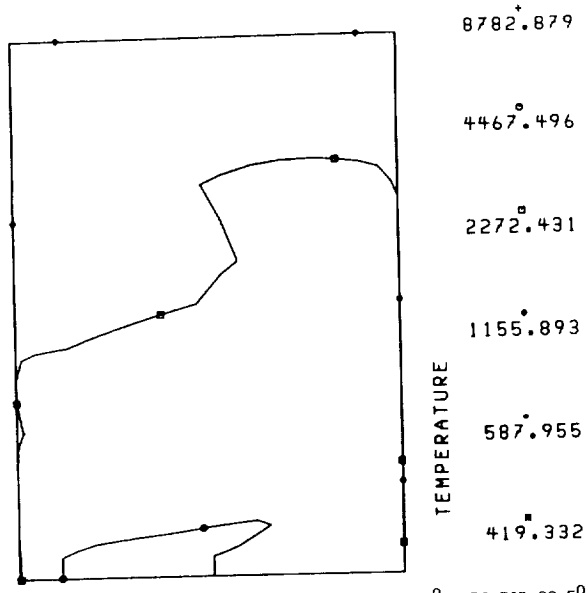

FIGURE 13. - TEMPERATURE ISOCONTOURS AT 358^{0} ATDC FOR 22.5^{0} SWIRL ANGLE.

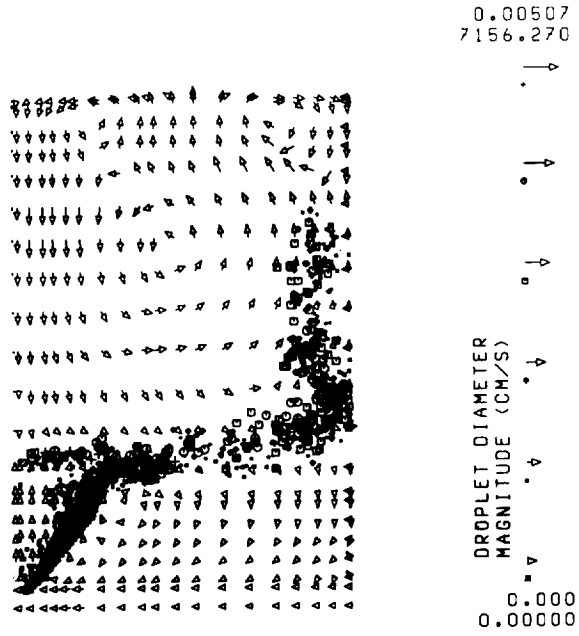

FIGURE 14. - GAS PHASE VELOCITY VECTOR PROFILES AND DROPLET LOCATIONS AT 359^{0} ATDC FOR 22.5^{0} SWIRL ANGLE.

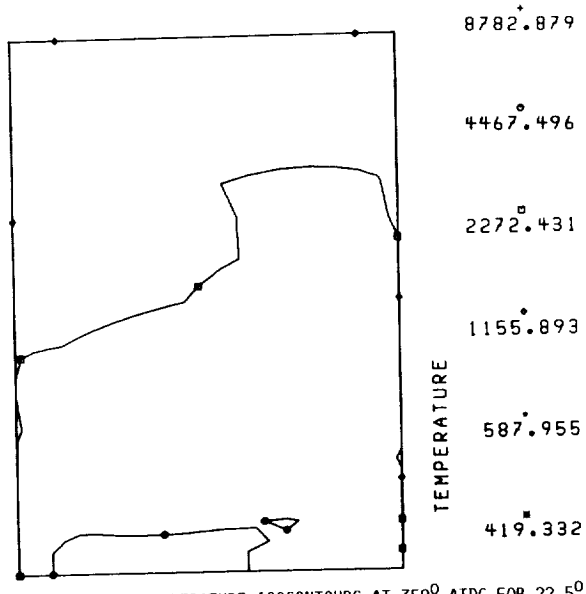

FIGURE 15. - TEMPERATURE ISOCONTOURS AT 359^{0} ATDC FOR 22.5^{0} SWIRL ANGLE.

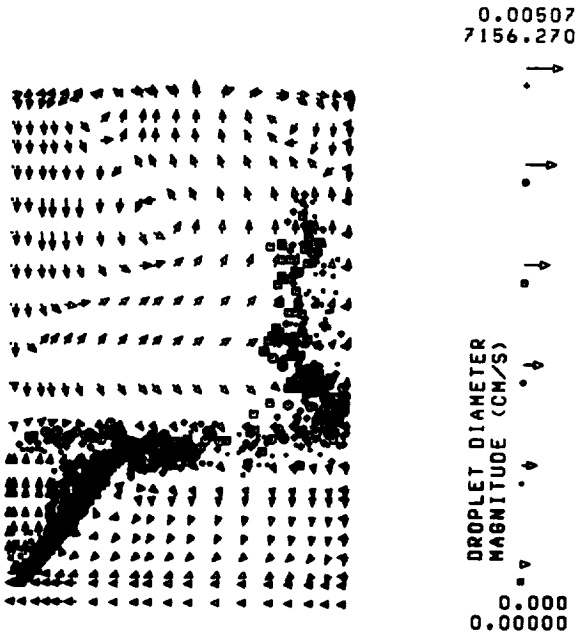

FIGURE 16. - GAS PHASE VELOCITY VECTOR PROFILES AND DROPLET LOCATIONS AT 360° ATDC FOR 22.5° SWIRL ANGLE.

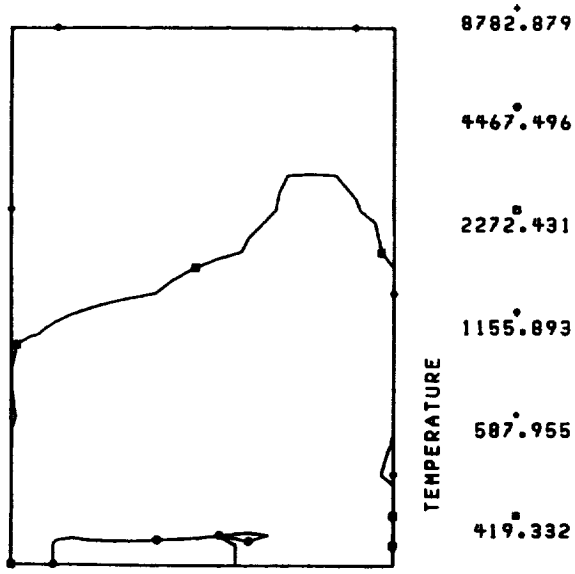

FIGURE 17. - TEMPERATURE ISOCONTOURS AT 360° ATDC FOR 22.5° SWIRL ANGLE.

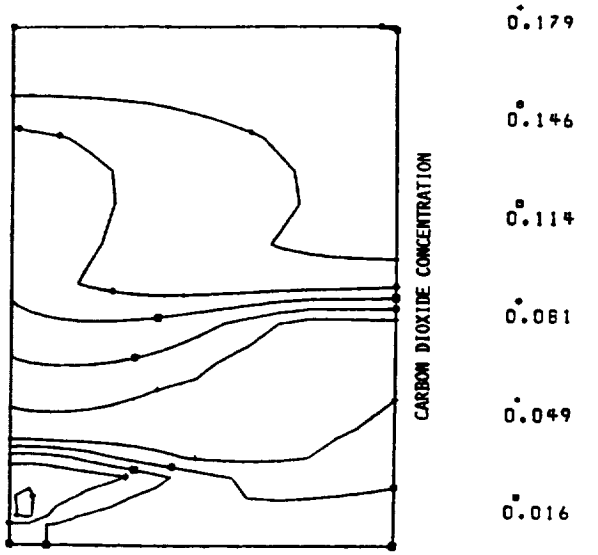

FIGURE 18. - CARBON DIOXIDE MASS FRACTION DISTRIBUTIONS AT 360° ATDC FOR 22.5° SWIRL ANGLE.

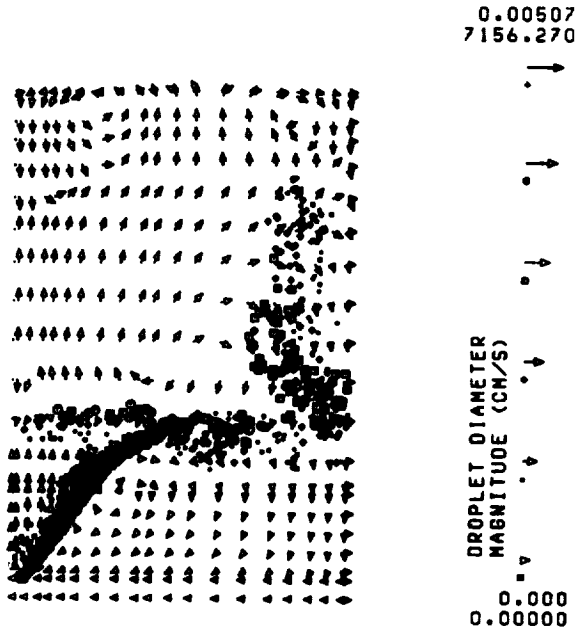

FIGURE 19. - GAS PHASE VELOCITY VECTOR PROFILES AND DROPLET LOCATIONS AT 1° ATDC FOR 22.5° SWIRL ANGLE.

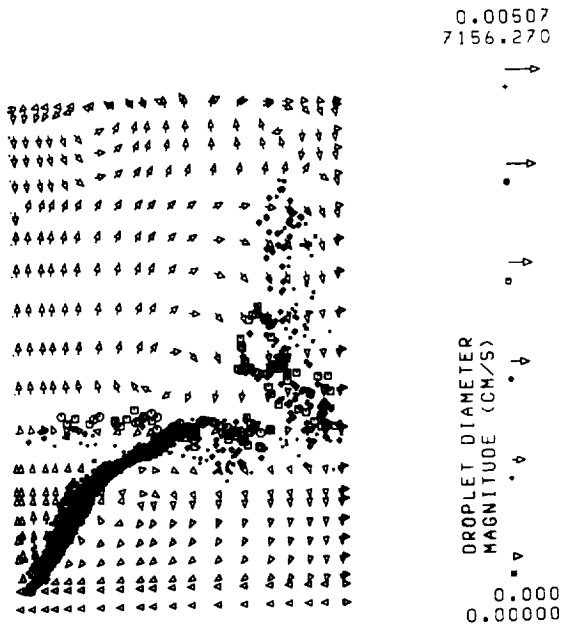

FIGURE 20. - GAS PHASE VELOCITY VECTOR PROFILES AND DROPLET LOCATIONS AT 2^{O} ATDC FOR 22.5^{O} SWIRL ANGLE.

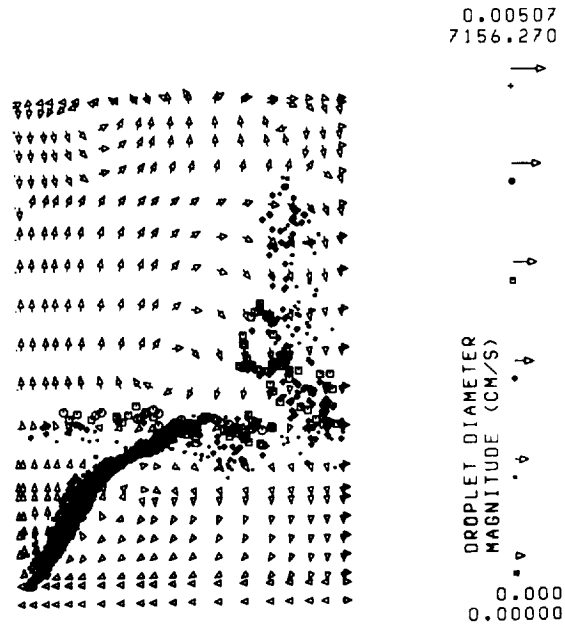

FIGURE 21. - GAS PHASE VELOCITY VECTOR PROFILES AND DROPLET LOCATIONS AT 3^{O} ATDC FOR 22.5^{O} SWIRL ANGLE.

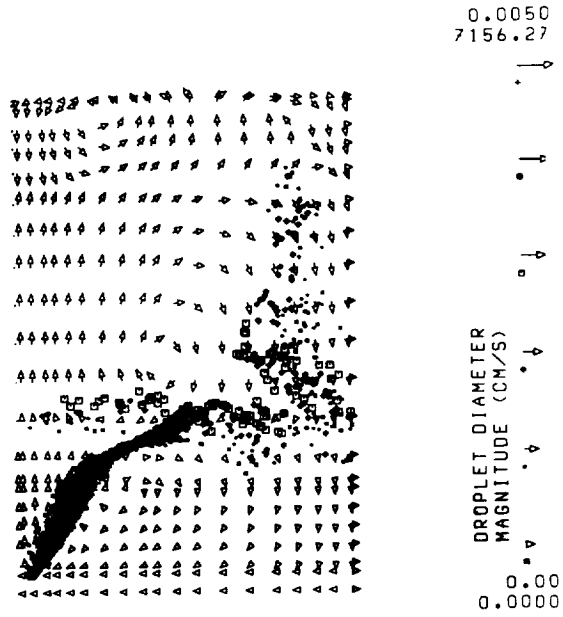

FIGURE 22. - GAS PHASE VELOCITY VECTOR PROFILES AND DROPLET LOCATIONS AT 4^{O} ATDC FOR 22.5^{O} SWIRL ANGLE.

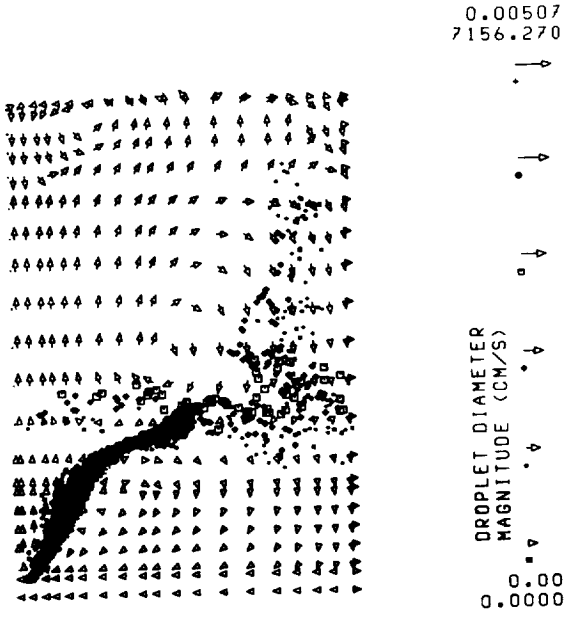

FIGURE 23. - GAS PHASE VELOCITY VECTOR PROFILES AND DROPLET LOCATIONS AT 5^{O} ATDC FOR 22.5^{O} SWIRL ANGLE.

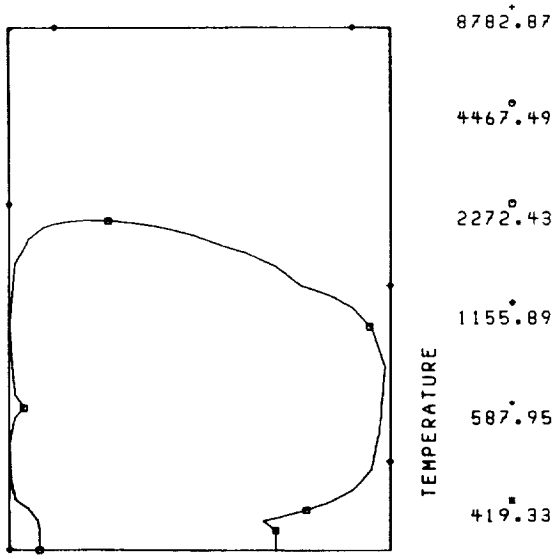

FIGURE 24. - TEMPERATURE ISOCONTOURS AT 5^0 ATDC FOR 22.5^0 SWIRL ANGLE.

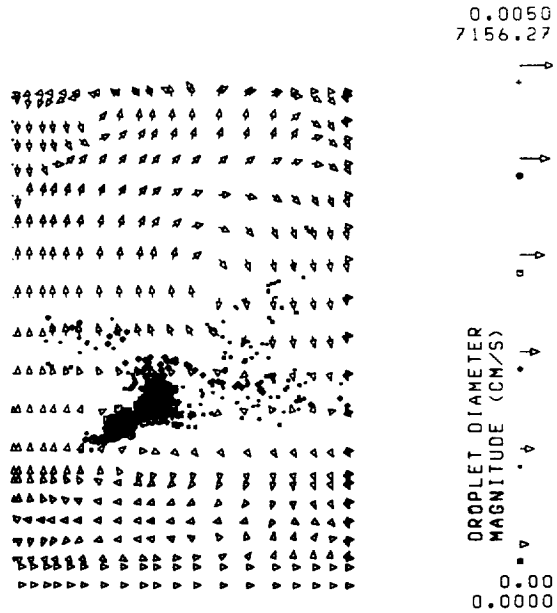

FIGURE 25. - GAS PHASE VELOCITY VECTOR PROFILES AND DROPLET LOCATIONS AT 10^0 ATDC FOR 22.5^0 SWIRL ANGLE.

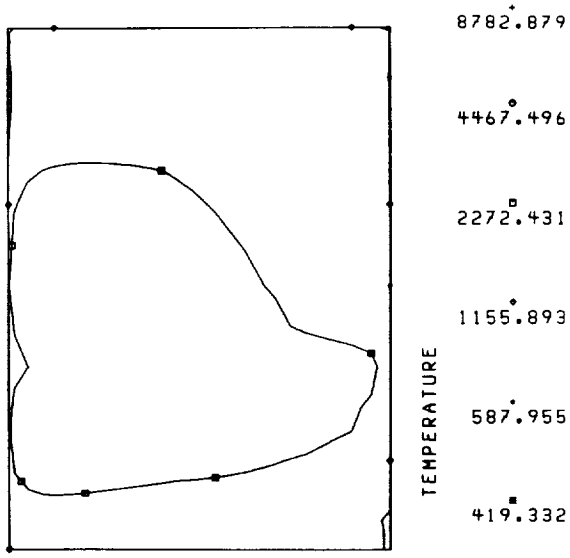

FIGURE 26. - TEMPERATURE ISOCONTOURS AT 10^0 ATDC FOR 22.5^0 SWIRL ANGLE.

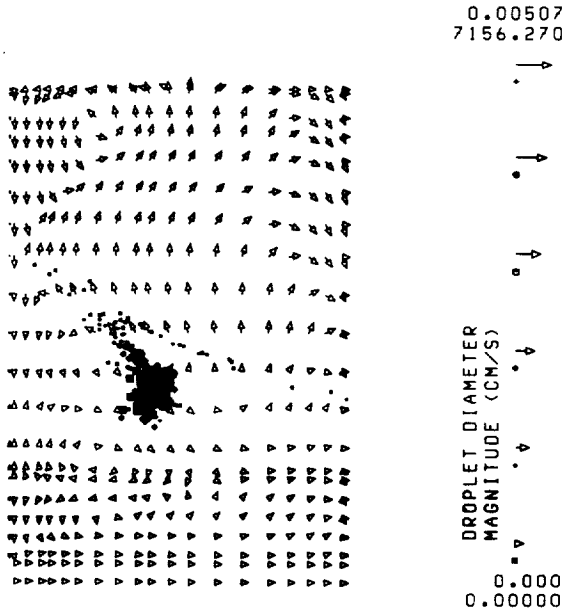

FIGURE 27. - GAS PHASE VELOCITY VECTOR PROFILES AND DROPLET LOCATIONS AT 15^0 ATDC FOR 22.5^0 SWIRL ANGLE.

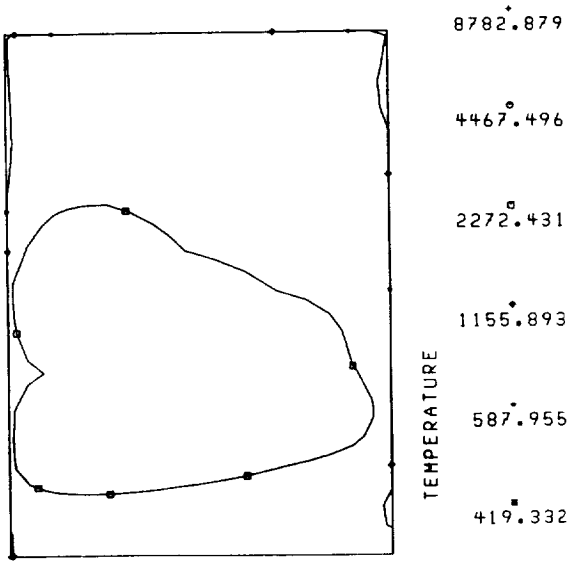

FIGURE 28. - TEMPERATURE ISOCONTOURS AT 15^0 ATDC FOR 22.5^0 SWIRL ANGLE.

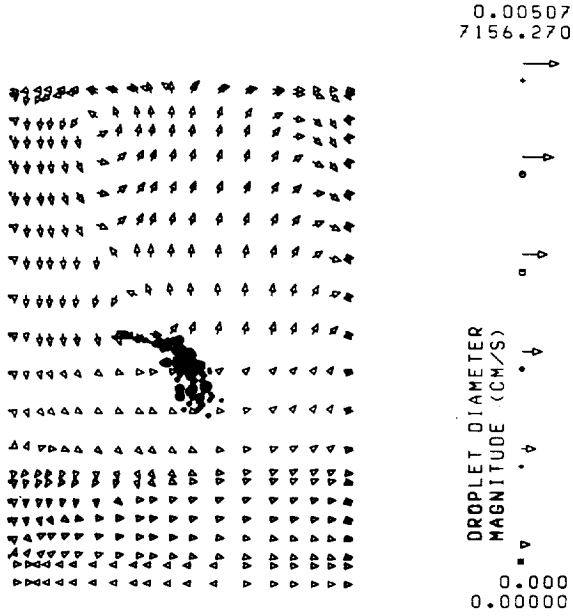

FIGURE 29. - GAS PHASE VELOCITY VECTOR PROFILES AND DROPLET LOCATIONS AT 20^0 ATDC FOR 22.5^0 SWIRL ANGLE.

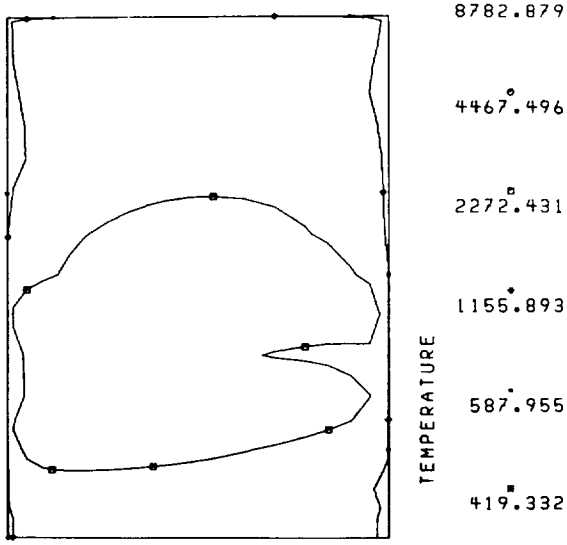

FIGURE 30. - TEMPERATURE ISOCONTOURS AT 20^0 ATDC FOR 22.5^0 SWIRL ANGLE.

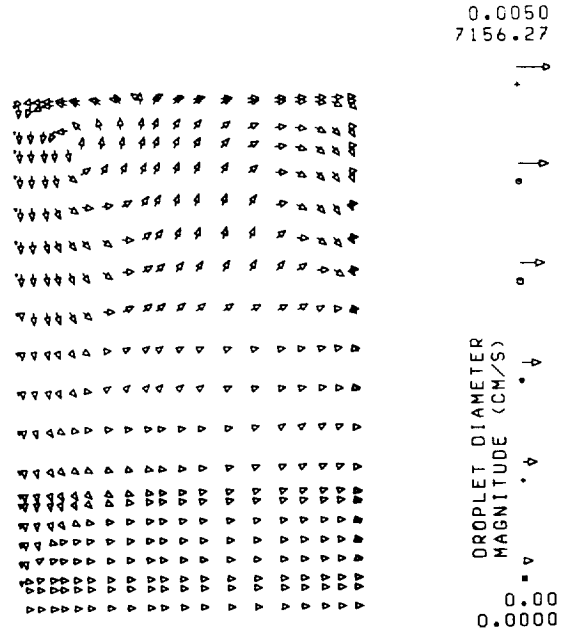

FIGURE 31. - GAS PHASE VELOCITY VECTOR PROFILES AND DROPLET LOCATIONS AT 30^0 ATDC FOR 22.5^0 SWIRL ANGLE.

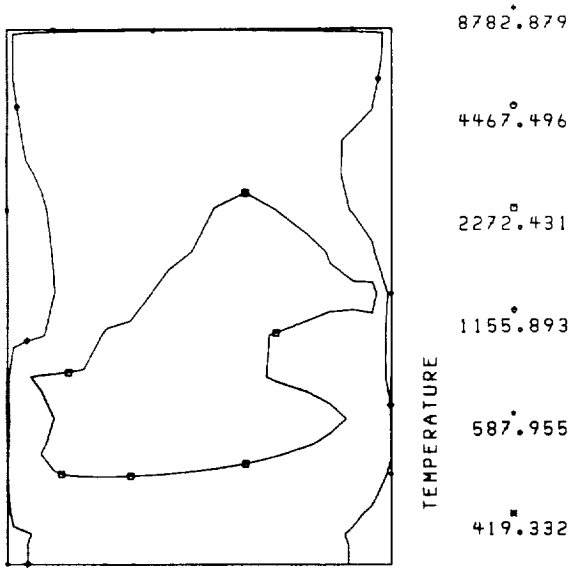

FIGURE 32. - TEMPERATURE ISOCONTOURS AT 30^0 ATDC FOR 22.5^0 SWIRL ANGLE.

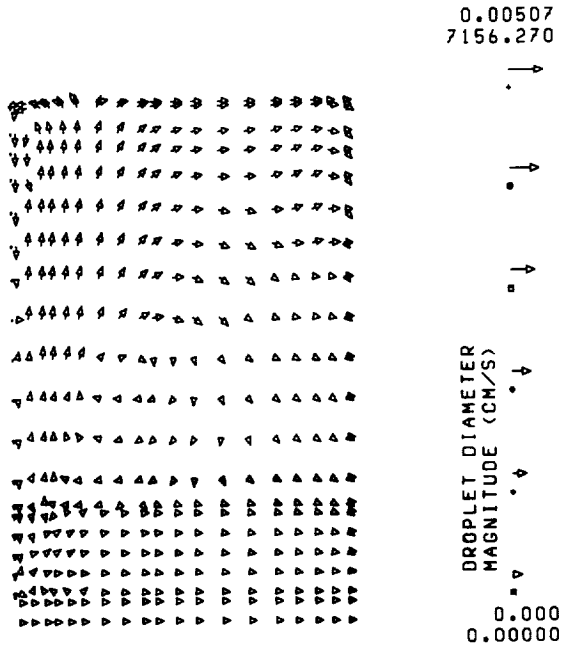

FIGURE 33. - GAS PHASE VELOCITY VECTOR PROFILES AT 40^0 ATDC FOR 22.5^0 SWIRL ANGLE.

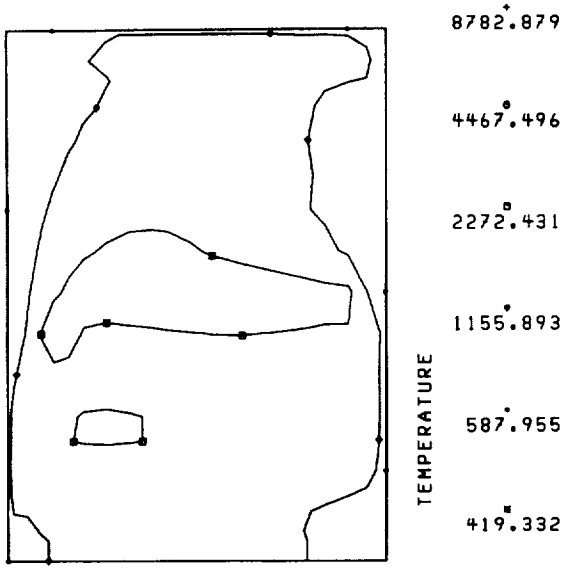

FIGURE 34. - TEMPERATURE ISOCONTOURS AT 40^0 ATDC FOR 22.5^0 SWIRL ANGLE.

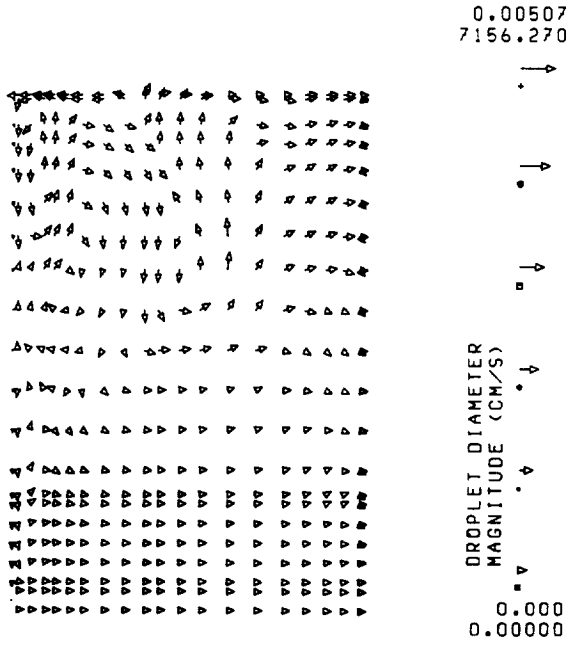

FIGURE 35. - GAS PHASE VELOCITY VECTOR PROFILES AT 60^0 ATDC FOR 22.5^0 SWIRL ANGLE.

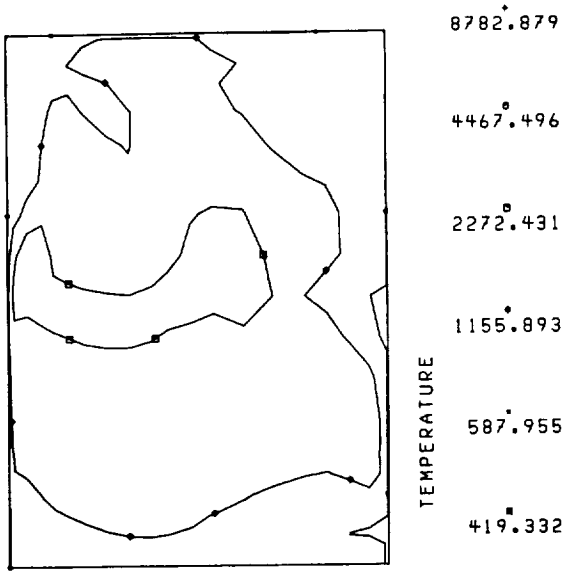

FIGURE 36. - TEMPERATURE ISOCONTOURS AT 60° ATDC FOR 22.5° SWIRL ANGLE.

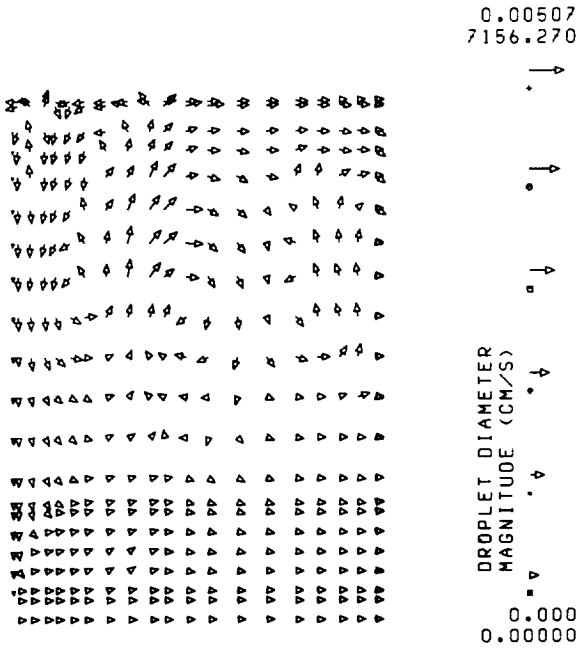

FIGURE 37. - GAS PHASE VELOCITY VECTOR PROFILES AT 80° ATDC FOR 22.5° SWIRL ANGLE.

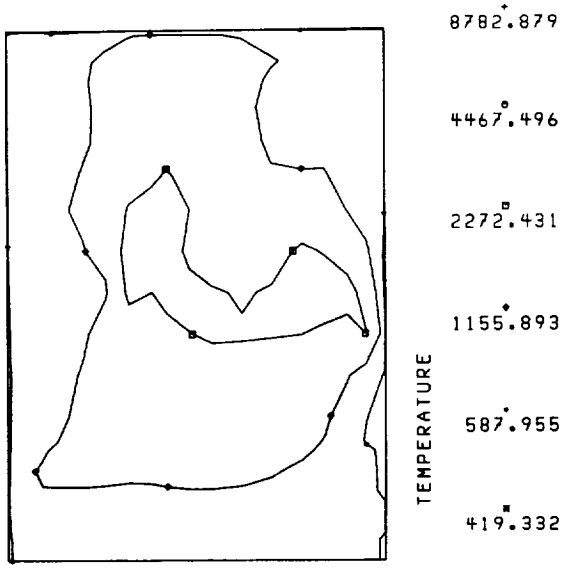

FIGURE 38. - TEMPERATURE ISOCONTOURS AT 80° ATDC FOR 22.5° SWIRL ANGLE.

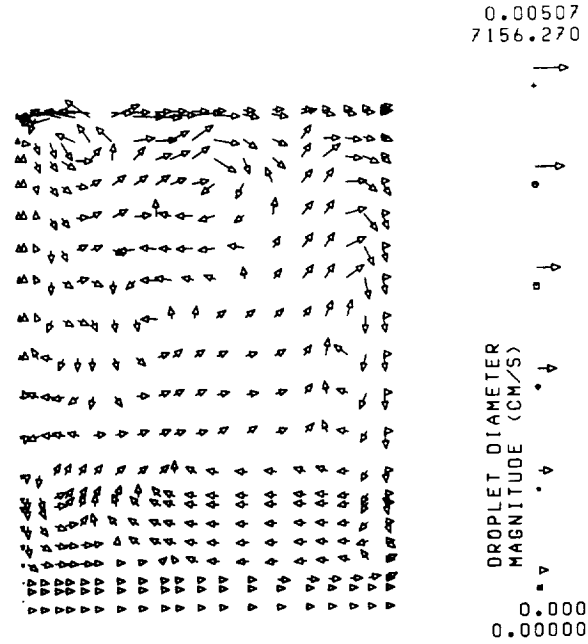

FIGURE 39. - GAS PHASE VELOCITY VECTOR PROFILES AT 108° ATDC FOR 22.5° SWIRL ANGLE.

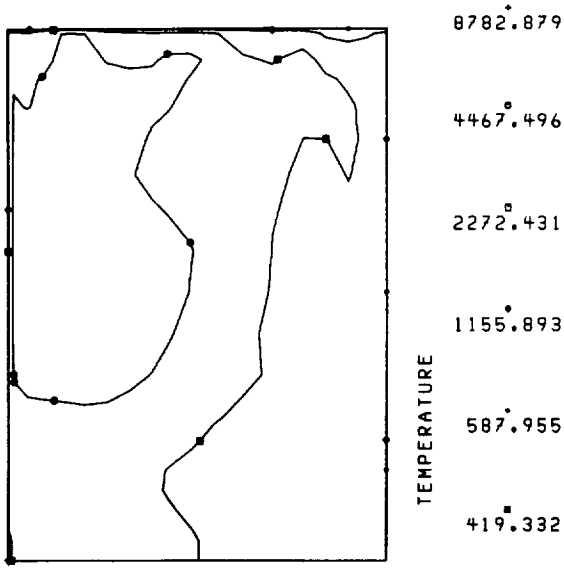

FIGURE 40. - TEMPERATURE ISOCONTOURS AT 108° ATDC FOR 22.5° SWIRL ANGLE.

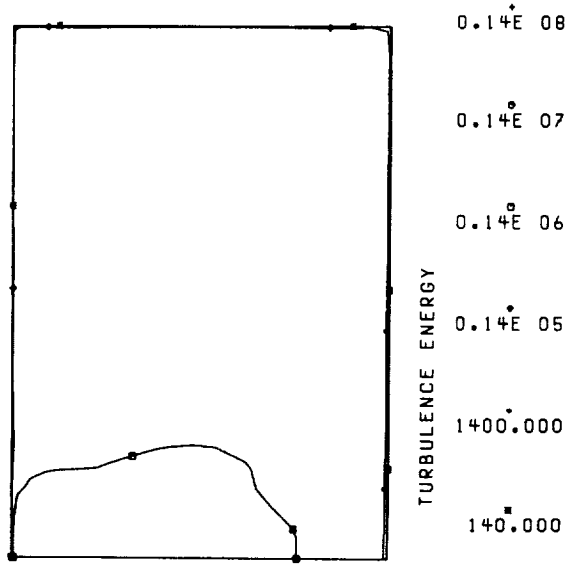

FIGURE 41. - NATURAL LOGARITHM OF TURBULENT KINETIC ENERGY PROFILES AT 350° ATDC FOR 22.5° SWIRL ANGLE.

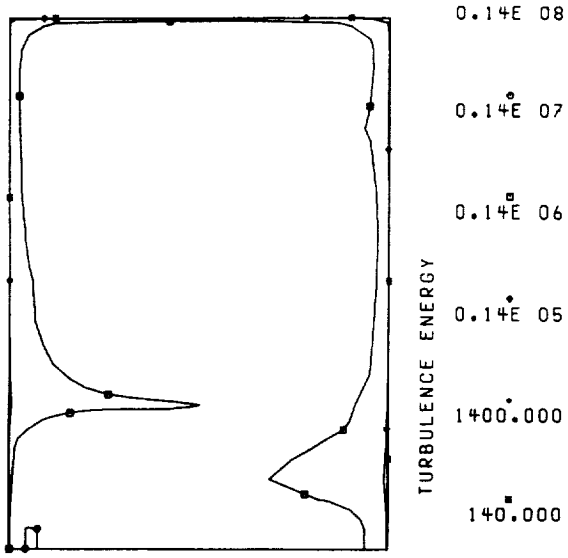

FIGURE 42. - NATURAL LOGARITHM OF TURBULENT KINETIC ENERGY ENERGY PROFILES AT 360° ATDC FOR 22.5° SWIRL ANGLE.

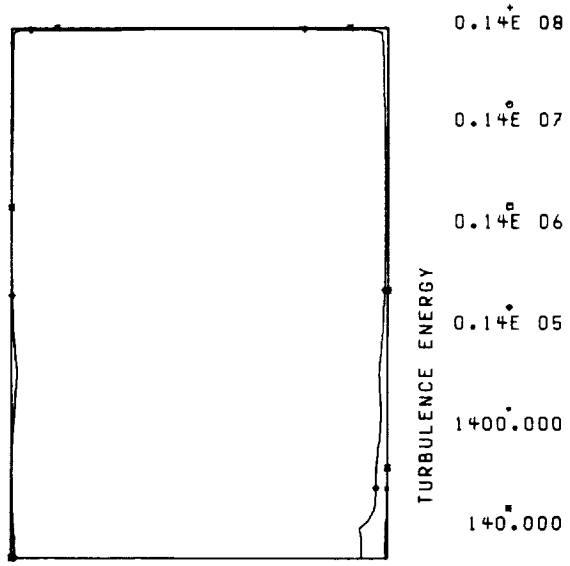

FIGURE 43. - NATURAL LOGARITHM OF TURBULENT KINETIC ENERGY PROFILES AT 10° ATDC FOR 22.5° SWIRL ANGLE.

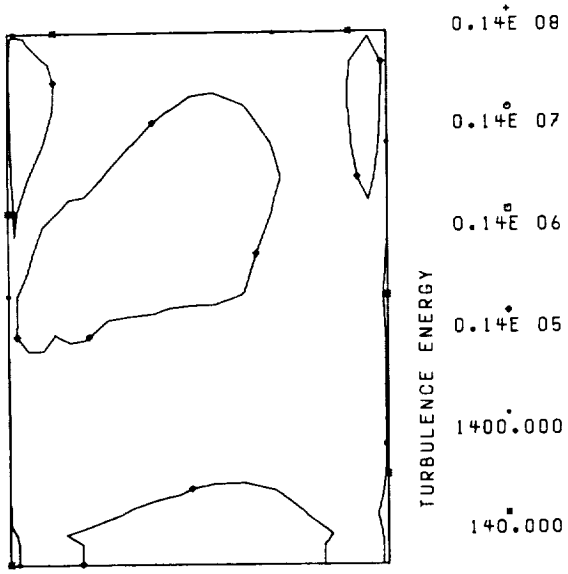

FIGURE 44. - NATURAL LOGARITHM OF TURBULENT KINETIC ENERGY PROFILES AT 40^{0} ATDC FOR 22.5^{0} SWIRL ANGLE.

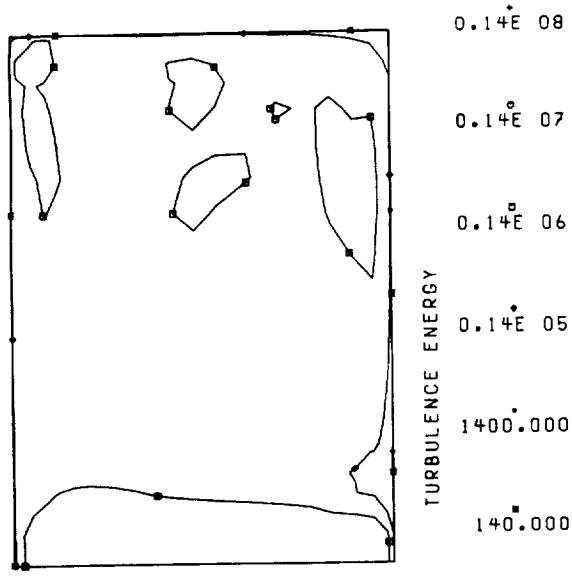

FIGURE 45. - NATURAL LOGARITHM OF TURBULENT KINETIC ENERGY PROFILES AT 108^{0} ATDC FOR 22.5^{0} SWIRL ANGLE.

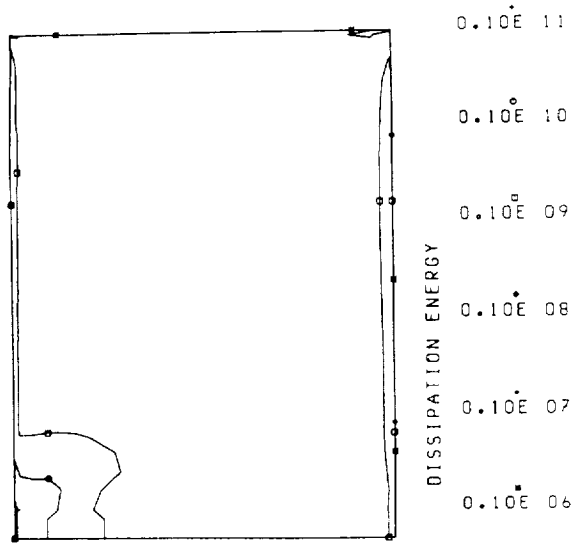

FIGURE 46. - NATURAL LOGARITHM OF DISSIPATION RATE OF TURBULENCE KINETIC ENERGY AT 350^{0} ATDC FOR 22.5^{0} SWIRL ANGLE.

NASA
National Aeronautics and Space Administration

Report Documentation Page

1. Report No.	2. Government Accession No.	3. Recipient's Catalog No.
NASA TM-102069		

4. Title and Subtitle

Two-Dimensional Analysis of Two-Phase Reacting Flow in a Firing Direct-Injection Diesel Engine

5. Report Date

December 1989

6. Performing Organization Code

7. Author(s)

H. Lee Nguyen

8. Performing Organization Report No.

E-4826

10. Work Unit No.

505-62-61

9. Performing Organization Name and Address

National Aeronautics and Space Administration
Lewis Research Center
Cleveland, Ohio 44135-3191

11. Contract or Grant No.

13. Type of Report and Period Covered

Technical Memorandum

12. Sponsoring Agency Name and Address

National Aeronautics and Space Administration
Washington, D.C. 20546-0001

14. Sponsoring Agency Code

15. Supplementary Notes

16. Abstract

This report describes a study of the flow field, spray penetration, vaporization, and combustion in two-stroke diesel engines. Fuel injection begins at 345° after top dead center (ATDC), and n-dodecane is used as the liquid fuel. Arrhenius kinetics is used to calculate the reaction rate term in the quasi-global combustion model. When the temperature, fuel, and oxygen mass fraction are within suitable flammability limits, combustion begins spontaneously. No spark is necessary to ignite a localized high-temperature region. Compression is sufficient to increase the gaseous phase temperature to a point where spontaneous chemical reactions occur. Results are described for a swirl angle of 22.5°.

17. Key Words (Suggested by Author(s))	18. Distribution Statement
2-dimensional two-phase reacting flow Two-stroke direct injection diesel engine Combustion	Unclassified – Unlimited Subject Category 07

19. Security Classif. (of this report)	20. Security Classif. (of this page)	21. No of pages	22. Price*
Unclassified	Unclassified	20	A03

NASA FORM 1626 OCT 86

*For sale by the National Technical Information Service, Springfield, Virginia 22161